# Corner collision implies border-collision bifurcation

M. di Bernardo*, C.J. Budd† and A.R. Champneys‡§

Submitted to Physica D March 20, 2000

*PACS*: 05.45.+b, 02.30.Hq, 03.20.+i, 84.30.Ng

*Keywords*: bifurcation; piecewise-smooth; border-collision; Poincaré map.

**Abstract**

This paper analyses a so-called *corner-collision* bifurcation in piecewise-smooth systems of ordinary differential equations (ODEs), for which a periodic solution grazes with a corner of the discontinuity set. It is shown under quite general circumstances that this leads to a normal form that is to lowest order a piecewise-linear map. This is the first generic derivation from ODE theory of the so called $C$-bifurcation (or border-collision) for piecewise-linear maps. The result contrasts with the equivalent results when a periodic orbit grazes with a smooth discontinuity set, which has recently been shown to lead to maps that have continuous first derivatives but not second.

Moreover, it is shown how to calculate the piecewise-linear map for arbitrary dimensional systems, using only properties of the single periodic trajectory undergoing corner collision. The calculation is worked out for two examples, including a model for a commonly used power electronic converter where complex dynamics associated with corner-collision was previously found numerically, but is explained analytically here for the first time.

## 1 Introduction

### 1.1 Preliminaries

Piecewise smooth (PWS) systems are an important class of ordinary differential equations (ODEs) whose dynamics are known to exhibit complex bifurcation scenarios and chaos. Here PWS refers to a dynamical system whose phase space can be divided into regions of smooth dynamics separated by finitely many codimension-one boundaries. Examples arise naturally in power electronic converters, relay control, vibro-impacting systems, models for stick slip motion with friction and many other physical processes. See, for example, the reference lists in the recent work Dankowitz & Nordmark (1999) and di Bernardo, Feigin, Hogan & Homer (1999). Broadly speaking, PWS systems can undergo all the bifurcations that smooth ones can, often far more dramatically, because discontinuities or jumps in the vector field represent a gross form of nonlinearity. More interestingly, there is a whole class of bifurcations that are unique to PWS systems, such as *grazings* (Nordmark 1991, Chin, Ott, Nusse & Grebogi 1994, Budd & Dux 1995), *chattering* (Budd & Dux 1994), and transitions to *sliding motion* (di Bernardo, Johansson & Vasca 1999, Filippov 1988).

Each of these bifurcations — grazing, chattering or onset of sliding — involve degenerate contact with a boundary. Specifically, suppose locally that one writes the phase space as $\mathcal{D} =$

*Department of Engineering Mathematics, University of Bristol BS8 1TR U.K. m.dibernardo@bris.ac.uk

†School of Mathematical Sciences, University of Bath BA2 7AY U.K. cjb@maths.bath.ac.uk

‡Department of Engineering Mathematics, University of Bristol BS8 1TR U.K. a.r.champneys@bris.ac.uk

§Corresponding author.

$S_1 \cup S_2 \cup \Sigma \subset \mathbb{R}^n$, where $\Sigma$ is an $(n-1)$-dimensional boundary separating regions $S_1$ and $S_2$ in which the dynamics is smooth. Assume that there exists a smooth limiting trajectory (such as a periodic orbit or a chaotic orbit in an $\omega$-limit set) that lies locally entirely in $S_1$. As we vary a parameter, there will typically be a first value at which this trajectory intersects $\Sigma$. If $\Sigma$ is itself smooth, then this will be a point of tangency, and in the case that $\Sigma$ is not locally simultaneously attracting (or repelling) from both sides $S_1$ and $S_2$, a grazing bifurcation occurs. This paper specifically concerns the case where $\Sigma$ is not smooth, which problems naturally arise in switching circuits in power electronics.

It is known (see the references in the next subsection) that such a grazing intersection can cause a dramatic qualitative change in the nature of the attractor. The aim of this paper is to demonstrate that a similar dramatic qualitative change occurs when the intersection occurs at a non-smooth point of $\Sigma$ and to classify the form that this change takes. For simplicity we confine our analysis to the case where the limiting trajectory is a hyperbolic periodic orbit, and derive the local form of the Poincaré map close to it. However the analysis can easily be extended (cf. Lamba (1995)) to other examples of limit trajectories. Our main result will be to show that locally the Poincaré map is piecewise linear (see for example Figures 8, 10 and 11 below).

### 1.2 Grazing and piecewise-linear maps

For regular grazing bifurcations, when $\Sigma$ is taken to be a smooth manifold, a complete characterization of what may ensue under parameter variation depends crucially on what is assumed about the order of smoothness of the vector field across $\Sigma$. A particular case of historical importance is that of a second-order forced oscillator that either impacts with a rigid wall (Thompson & Ghaffari 1983, Shaw & Holmes 1983*b*) or undergoes a change in stiffness or damping constant on passing though some spatial location (Thompson, Bokaian & Ghaffari 1983, Shaw & Holmes 1983*a*). The impacting case, for which the vector field has a delta-function-type discontinuity given by a restitution law, has been shown to lead to dynamics associated with a one-dimensional map that has a square-root singularity (Nordmark (1991, 1997)). Such maps are known to undergo period-adding sequences and chaotic dynamics associated with 'fingered' strange attractors. The other cases, for which the vector field is at least bounded and often continuous across the boundary, have yet to be analysed as completely. Recently, in the course of analyzing a model for stick-slip oscillations, Dankowitz & Nordmark (1999) rigorously derived a local *discontinuity map* (DM), a normal form which describes dynamics in the neighbourhood of a grazing bifurcation, for an arbitrary autonomous vector field which is continuous across the boundary. Such maps are locally differentiable at the grazing bifurcation but have an order-3/2 singularity. Work by the present authors (di Bernardo, Budd & Champneys 2000*b*) extends this result, using formal power series expansions, to deal with arbitrary grazing bifurcations including the case of discontinuity of the vector field. The conditions defining grazing in a discontinuous vector field are more subtle, since one has to avoid the possibility of sliding solutions when the discontinuity surface is attracting from both sides; see e.g. di Bernardo, Johansson & Vasca (1999). Also, we show in di Bernardo, Budd & Champneys (2000*a*) for the special case of second-order oscillators, how the local DM relates to the global properties of the Poincaré map away from the corner collision. For example this elucidates why, in the limit of large stiffness ratios, a bilinear oscillator behaves very much like an impact oscillator (e.g. cf. Chapters 14 and 15 of Thompson & Stewart (1986)), even though the local DMs are very different.

In parallel with the literature on grazings for systems of ODEs, have been bifurcation theory results for iterated maps which are locally piecewise linear. Such were termed $C$-bifurcations in the work of Feigin starting with (Feigin 1970) (see di Bernardo, Feigin, Hogan & Homer (1999) for a modern review) who undertook a classification of the existence of various periodic orbits in the neighbourhood of the analogue of a grazing bifurcation for such a map. That is, as a parameter varies, a fixed point of the map passes through the border between the two different linear pieces.

Depending on calculable details of the map in each piece, one can have for instance the change of stability of a periodic orbit, the merging of two orbits, the transition from a stable period-1 orbit to a stable period-$n$ orbit *for any* $n$, or the sudden transition to a chaotic attractor. Feigin's work on $C$-bifurcation was independently re-derived by Nusse, Ott & Yorke (1994), where it was given the name 'border collision', see also Nusse & Yorke (1995) and Banerjee & Grebogi (1999). They extended the analysis to propose a classification of all two-dimensional maps undergoing border-collision by reduction to a normal form map with a minimal number of calculable coefficients. It has also recently been shown by Banerjee, York & Grebogi (1999) that the dynamics of such maps may feature so-called *robust* chaotic dynamics without parameter windows of periodic behaviour.

The missing step in the literature at present seems to be the derivation of $C$-bifurcations and piecewise-linear maps directly from ODEs. It is appealing to argue, as in di Bernardo, Feigin, Hogan & Homer (1999), that grazing bifurcations for continuous but non-differentiable vector fields should lead to piecewise-linear maps since one can meaningfully linearize around a periodic orbit on either side of the parameter value at which it grazes. However, the situation is more subtle and a careful analysis of grazing in this case (Dankowitz & Nordmark 1999, di Bernardo et al. 2000*b*) leads to maps that are locally differentiable with a an order-3/2 singularity. Hence, at least at the very local level, grazings and border-collision bifurcations are *not* the same. An apparent contradiction, is the planar example (di Bernardo, Feigin, Hogan & Homer 1999, Sect. 7) that was analytically derived by Feigin as the flow whose Poincaré map is exactly composed of two linear pieces. A careful examination reveals that this system is in fact a system of non-local (delay) differential equation with a discontinuous delay term. Therefore this example does not satisfy the typical hypotheses for grazing bifurcations in ODEs.

### 1.3 Corners and corner collisions

As already mentioned, a basic hypothesis usually assumed for grazing is that the discontinuity boundary $\Sigma$ itself should be a smooth subset of phase space. However, in applications for example to control systems and electronic switching devices, this may not be the case if a number of different switching scenarios are governed by several overlapping inequalities. A generic feature of such examples is that the discontinuity boundary has a corner-type singularity formed by the intersection between smooth codimension-one surfaces $\Sigma_1$ and $\Sigma_2$ at a non-zero angle. The locus of corners $\mathcal{C}$ will in general be a $(n-2)$-dimensional subset of $\mathbb{R}^n$. The passage of a trajectory through a point in $\mathbf{c} \in \mathcal{C}$ is a bifurcation event because, in a neighbourhood of the corner, there will generically be topologically distinct trajectories that do not behave similarly with respect to regions $S_1$ and $S_2$. If such a trajectory is an isolated periodic orbit $\mathbf{p}(t)$, we shall refer to this as a *corner collision* bifurcation. Figure 1 illustrates the geometry that we are considering.

There are two generic kinds of such intersections between a trajectory and $\mathcal{C}$ leading to differing bifurcations which we shall refer to either an *external* or *internal* corner collision. These are illustrated in Figure 2(a) and (b) respectively. The third possibility, depicted in Figure 2(c), we shall not refer to as a corner-collision because some trajectories in the neighbourhood of the corner-colliding one undergo sliding along a portion of the boundary. This situation would lead to entirely different dynamics and its analysis is left to future work.

Given necessary conditions (to be specified in Section 2 below) which preclude case (c) of Figure 2, then a sufficient condition for a corner-collision to occur is just that a periodic orbit $\mathbf{p}(t)$ intersects the codimension-two corner manifold $\mathcal{C}$. Since we can choose the phase of $p$ for which this happens, a corner-collision is thus a codimension-one bifurcation. Contrast this with a grazing bifurcation with a smooth boundary. Here one requires not only that $\mathbf{p}(t)$ intersects the codimension-one discontinuity boundary $\Sigma$, but additionly that the vector field be tangent to $\Sigma$ (both from the side $S_1$ and $S_2$) at this point. This is an extra codimension-one constraint, meaning that grazing bifurcations are also of codimension one. Hence a periodic orbit grazing with a smooth boundary and passage through the corner are equally likely events, both being

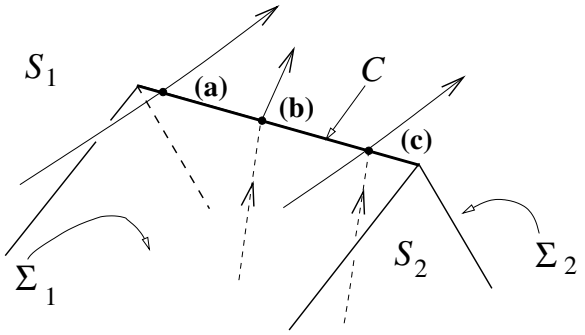


Figure 1: *The geometry of the corner depicted in three dimensions. Here the discontinuity boundary is composed locally of two* $(n-1)$*-dimensional manifolds* $\Sigma_1$ *and* $\Sigma_2$ *which intersect along the* $(n-2)$*-dimensional corner manifold* $\mathcal{C}$*. Three trajectories (a),(b),(c) (corresponding to the respective panels of Figure 2 below) are plotted which highlight topologically distinct forms of interaction with the corner. Cases (a) and (b) represent internal and external corner collision respectively, whereas (c) is not a corner collision as defined here, since there is non-uniqueness in reverse time. In this and subsequent pictures, trajectory segments in* $S_1$ *are depicted by solid lines and those in* $S_2$ *by dashed lines.*

of codimension-one for a dissipative system. This article shall derive for the first time a local analysis of the latter.

The study of corner collision as a bifurcation in its own right has been motivated by recent studies on the dynamics of a certain class of DC-DC power electronic converters (di Bernardo, Budd & Champneys 1998, Yuan, Banerjee, Ott & Yorke 1998) in which the switching surface consists of a periodic saw-tooth signal, see Section 5.2 below for the details. Here it can be shown that grazing with the ramp part of the saw-tooth is impossible for a large range of parameter values, but that corner collision is not only possible but is instrumental in the transition from regular one-switch-per-period dynamics to chaotic dynamics involving skipped cycles and many switches per period. For the configuration studied in di Bernardo et al. (1998) the corner collision was numerically shown to be equivalent locally to a piecewise-linear map and this map was then shown to lead to saddle-node-type bifurcations that organize in a spiraling bifurcation diagram. In the configuration studied by Yuan et al. (1998), in which multiple switchings per period are prevented by means of a 'latch', the corner-collision causes an immediate jump to chaos. This jump was shown *a posteriori* to be describable by a border-collision normal form, after numerically extracting information from the simplest periodic orbits existing before and after the collision.

Thus we infer from the numerical calculations that corner-collision bifurcations in systems of ODEs leads in general to piecewise linear maps which undergo $C$-bifurcations (border collisions). The present paper is devoted to proving this statement analytically under the assumption that the vector field is discontinuous across a boundary which consists of a convex corner and that a periodic orbit undergoes an internal or an external corner collision. We shall give explicit formulae for computing the DM in a neighbourhood of the corner collision, which rely only on the geometry of the corner and linearization about the corner-colliding periodic orbit. In fact the major part of this analysis is to compute a local DM that describes the dynamics in a small neighbourhood of the corner. The form of this local mapping does not rely on $\mathbf{p}(t)$ being a periodic orbit, and is thus applicable to more general invariant sets, not just periodic orbits, which undergo corner collision. We shall also treat two example systems including the aforementioned DC-DC converter, showing analytically for the first time the existence of both external and internal corner collision bifurcations based only on the numerical computation of a single periodic orbit in each case. The other example is a planar ODE system that can be solved in closed form. For both examples, the analytical DM is shown to perfectly match the numerical or analytical solution of the ODEs.

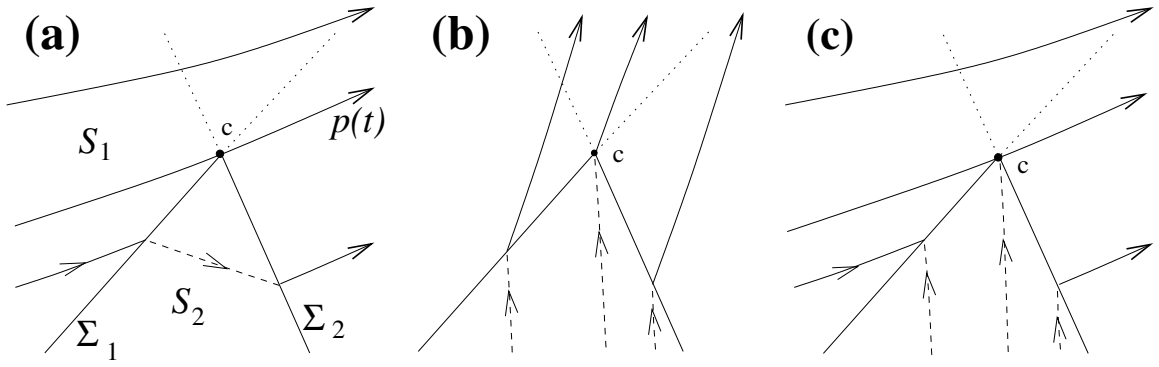


Figure 2: *Illustrating, in a general two-dimensional slice, trajectories in the neigbourhood of the three types of interaction with the corner depicted in Figure 1:* **(a)** *external corner-collision;* **(b)** *internal; and* **(c)** *which is not a corner-collision as defined in this paper. Note the topological difference between cases (a) and (b). In the latter, all trajectories enter both regions $S_1$ and $S_2$, whereas in the former, some trajectories remain locally in $S_1$. Case (c) fails the hypotheses of a corner-collision bifurcation, because the left-hand portion of the boundary, $\Sigma_1 = 0$ is attracting from both sides and hence sliding solutions would occur.*

### 1.4 Outline

The rest of the paper is outlined as follows. First we treat the case of external corner collision. Section 2 undertakes an analysis in a neighbourhood of the corner to compute the local discontinuity mapping. Two different maps are derived, one to compute the effect of passage through the corner taking zero time, and the other to compute the effect on a mapping derived via a Poincaré section. Section 3 then couples this local map to a global one derived from linearization about the periodic orbit globally, away from the corner. Section 4 then treats internal corner collision, showing that, even though it is topologically different from the external case, its analysis is, in effect, identical. Section 5 treats the examples, first the explicitly solvable one and then the buck converter. Finally Section 6 draws conclusions.

## 2 Local analysis near an external corner collision

We now consider a local analysis of the behaviour of trajectories in the neighbourhood of an external corner colliding trajectory $\mathbf{p}(t)$ (as illustrated in Figure 2(a)). We do not assume at this stage that $\mathbf{p}(t)$ is part of a periodic orbit. Suppose that a sufficiently small neighbourhood $\mathcal{D} \subset \mathbb{R}^n$ of the corner has been chosen so that the following description in terms of local coordinates is valid. $\mathcal{D}$ is divided into two regions $S_1$ where $\dot{\mathbf{x}} = \mathbf{F}_1$ and $S_2$ where $\dot{\mathbf{x}} = \mathbf{F}_2$, with the border $\Sigma$ between $S_1$ and $S_2$ which consisting of a triangular wedge when projected onto a general plane. This wedge is described by two smooth codimension-one surfaces $\Sigma_1$ and $\Sigma_2$ which are given by the zero sets of differentiable functions $H_1(\mathbf{x}) = 0$ and $H_2(\mathbf{x}) = 0$ in such a way that the system may be expressed as

$$\dot{\mathbf{x}} = \begin{cases} \mathbf{F}_2(\mathbf{x},t) & \text{if} \quad H_1(\mathbf{x}) < 0 \quad \text{and} \quad H_2(\mathbf{x}) < 0 \quad (\text{i.e. } \mathbf{x} \in S_2) \\ \mathbf{F}_1(\mathbf{x},t) & \text{otherwise} \qquad\qquad\qquad\quad (\text{i.e. } \mathbf{x} \in S_1) \end{cases}, \qquad \mathbf{x} \in \mathbb{R}^n. \tag{2.1}$$

This is illustrated in Figure 3. The sets $H_1 = 0$ and $H_2 = 0$ are assumed to intersect along a smooth codimension-two surface $\mathcal{C}$ (the corner) at a non-zero angle

$$\nabla H_1 \times \nabla H_2 \neq 0.$$

We suppose that $\mathbf{p}(t)$ locally lies entirely in region $S_1$ apart from a single point of intersection with the corner at a point $\mathbf{c} \in C$. Without loss of generality we assume that coordinates have

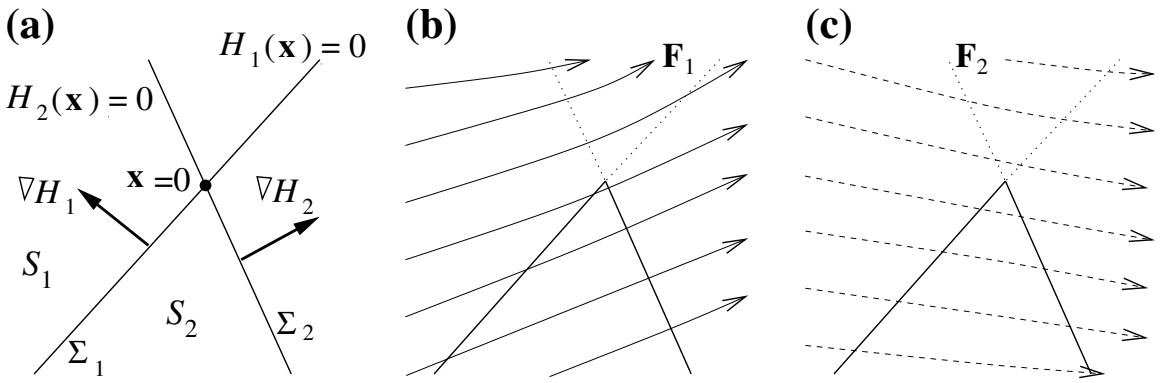


Figure 3: **(a)** *The geometry of the corner at an external corner collision.* **(b),(c)** *the vector fields* $\mathbf{F}_1$ *and* $\mathbf{F}_2$*, when extended to be defined in a full neighbourhood* $\mathcal{D}$ *of the corner.*

been chosen so that $\mathbf{c} = \mathbf{0}$. For such a corner-collision we shall refer to region $S_1$ as being the region *outside* the wedge defined by $\{H_1(\mathbf{x}) < 0,\ H_2(\mathbf{x}) < 0\}$, and $S_2$ as being *inside*. The functions $\mathbf{F}_1$ and $\mathbf{F}_2$ are assumed to be defined and sufficiently smooth (at least $C^2$) within a full neighbourhood of the origin. In particular both vector fields are well defined both inside and outside the wedge. (Also it is largely immaterial what is assumed for the vector field precisely on the boundaries $H_1 = 0$ or $H_2 = 0$, or at corner, provided the slope conditions (2.2) below are satisfied there).

Now we wish to describe trajectories close to the special trajectory $\mathbf{p}(t)$. In order to avoid sliding, we require certain slope conditions to be satisfied by the vector fields $\mathbf{F}_{1,2}$. With reference to Figure 3(c,d), the slope conditions for external grazing can easily be seen to be (without loss of generality up to a reversal of time if necessary)

$$\langle \mathbf{F}_i, \nabla H_1 \rangle < 0, \quad \langle \mathbf{F}_i, \nabla H_2 \rangle > 0, \quad \text{for} \quad i = 1, 2. \tag{2.2}$$

Since all constructions are local, and these are open conditions, it is sufficient to assume that the conditions (2.2) hold at $\mathbf{x} = \mathbf{0}$, the point of the intersection of $\mathbf{p}(t)$ with $\mathcal{C}$. Observe that we do not require that (2.2) hold at all points on $\mathcal{C}$. Indeed, as illustrated in Figure 2, different parts of $\mathcal{C}$ may satisfy the conditions for external or internal grazing, or may preclude corner-collision altogether.

## 2.1 The concept of a discontinuity map

Our aim is to describe a discontinuity mapping (DM) for trajectories close to $\mathbf{p}(t)$, in the spirit of Dankowitz & Nordmark (1999) whose analysis applies to the case of grazing with a smooth discontinuity surface. A DM is a local map that describes the correction that needs to be made to trajectories that pass through region $S_2$ close to $\mathbf{x} = \mathbf{0}$ in order to solve the global Poincaré map as if the wedge were not there. In the present setting, the analysis will be simpler because it will transpire that linear approximations to the flow are sufficient to determine the leading order terms of the DM. We shall consider two forms of DM, the zero-time map (ZDM) and the Poincaré-section version (PDM). The latter applies quite generally, but we shall begin with the former, which is a more direct analogy of the DM for smooth grazings derived by Dankowitz & Nordmark and applies specifically to the often encountered case of periodically forced systems.

Both mappings are derived by considering an approximation to the flows $\phi_1$ and $\phi_2$ defined by

$$\frac{\partial \phi_i}{\partial t} = \mathbf{F}_i(\phi_i(\mathbf{x}, t), t), \quad \phi_i(\mathbf{x}, 0) = \mathbf{x}, \quad i = 1, 2. \tag{2.3}$$

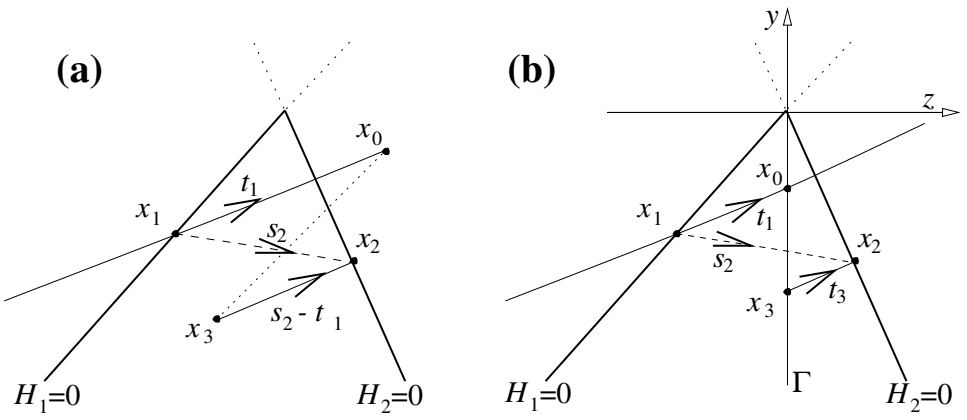


Figure 4: **(a)** *The ZDM takes* $\mathbf{x}_0$ *to* $\mathbf{x}_3$ *in zero time.* **(b)** *The PDM takes* $\mathbf{x}_0$ *to* $\mathbf{x}_3$ *in time* $s_2 - t_1 - t_3$.

Note that both flows are defined even on the 'wrong' side of the discontinuity surface. Expanding these flows about the corner-collision point $\mathbf{x} = \mathbf{0}$ at $t = 0$ we have

$$\phi_i(\mathbf{x}, t) = \mathbf{x} + \mathbf{F}_i^0 t + \left(\frac{\partial \mathbf{F}_i}{\partial \mathbf{x}}\right)^0 \left(\mathbf{x}t + \mathbf{F}_i^0 \frac{t^2}{2}\right) + o\left(\|\mathbf{x}\|^2, \|\mathbf{x}\|t, t^2\right), \tag{2.4}$$

where a superscript zero denotes a quantity evaluated at $\mathbf{x} = 0$, $t = 0$.

## 2.2 The zero-time discontinuity mapping (ZDM)

In order to construct a map that takes zero time, we need only consider trajectories that intersect the wedge. The DM for other trajectories will be the identity map. In what follows we shall refer to the dynamical systems corresponding to vector fields $\mathbf{F}_1$ and $\mathbf{F}_2$ defined on the whole of $\mathcal{D}$ as systems 1 and 2 respectively.

The ZDM is constructed as illustrated in Figure 4(a). In order to calculate the leading-order expression in a neighbourhood of $\mathbf{x} = \mathbf{0}$, it will transpire that the linear terms in (2.4) are sufficient to completely describe the dynamics. In order to show this, we shall keep track of the error term in what follows to ensure that is smaller than the leading order term given by the linear approximation. Specifically we want to

- solve system 1 starting at $\mathbf{x} = \mathbf{x}_0$ for time $-t_1$ until $\mathbf{x} = \mathbf{x}_1$ such that $H_1(\mathbf{x}_1) = 0$,
- then solve system 2 for time $s_2$ until $\mathbf{x} = \mathbf{x}_2$ such that $H_2(\mathbf{x}_2) = 0$,
- and finally solve system 1 again for time $t_1 - s_2$ calling the final point $\mathbf{x} = \mathbf{x}_3$.

The effect of such a computation will take zero time, and the resulting map from $\mathbf{x}_0$ to $\mathbf{x}_3$ represents the correction to trajectories of system 1 alone (if it applied in the whole of $\mathcal{D}$) in order to account for the time spent in region $S_2$ where system 2 applies.

By construction, $t_1$ is the unique local solution $T_1(\mathbf{x}_0)$ of $H_1(\phi_1(\mathbf{x}_0, -T_1(\mathbf{x}_0)) = 0$. Taking a Taylor expansion of $H_1$, expanding about $\mathbf{x} = 0$, $t = 0$, one obtains

$$\langle \nabla H_1^0, \mathbf{F}_1^0 \rangle (-T_1(\mathbf{x}_0)) + \langle \nabla H_1^0, \mathbf{x}_0 \rangle + o(|\mathbf{x}_0|, T_1) = 0. \tag{2.5}$$

Now by (2.2) one can divide by the scalar $\langle \nabla H_1^0, \mathbf{F}_1^0 \rangle$ and hence

$$T_1(\mathbf{x}_0) = \frac{\langle \nabla H_1^0, \mathbf{x}_0 \rangle}{\langle \nabla H_1^0, \mathbf{F}_1^0 \rangle} + o(|\mathbf{x}_0|), \tag{2.6}$$

where in order to write the error term we must assume that the local region around the corner has been chosen to be sufficiently small so that $\mathbf{x}_0 \ll \langle \nabla H_1^0, \mathbf{F}_1^0 \rangle$. Hence

$$\mathbf{x}_1 = \phi_1(\mathbf{x}_0, -T_1(\mathbf{x}_0)) = \mathbf{x}_0 - F_1^0 T_1(\mathbf{x}_0) + o(|\mathbf{x}_0|). \tag{2.7}$$

Similarly $s_2$ is defined as the unique local solution of $H(\phi_2(\mathbf{x}_1, S_2(\mathbf{x}_1)) = 0$. So that

$$S_2(\mathbf{x}_1) = -\frac{\langle \nabla H_2^0, \mathbf{x}_1 \rangle}{\langle \nabla H_2^0, \mathbf{F}_2^0 \rangle} + o(|\mathbf{x}_1|), \tag{2.8}$$

where again the slope assumptions (2.2) imply that the denominator is non-zero and here we assume that $\mathbf{x}_1 \ll \langle \nabla H_2^0, \mathbf{F}_2^0 \rangle$, and

$$\mathbf{x}_2 = \phi(\mathbf{x}_1, S_2(\mathbf{x}_1)) = \mathbf{x}_2 + \mathbf{F}_2^0 S_2(\mathbf{x}_1) + o(|\mathbf{x}_1|). \tag{2.9}$$

Finally, we have

$$\mathbf{x}_3 = \phi_1(\mathbf{x}_3, t_1 - s_2) = \mathbf{x}_2 + \mathbf{F}_1^0 \left( T_1(\mathbf{x}_0) - S_2(\mathbf{x}_1) \right) + o(\mathbf{x}_2).$$

Upon substitution from (2.6), (2.7), (2.8) and (2.9), this expression for $\mathbf{x}_3$ can be re-arranged to read

$$\mathbf{x}_3 = \mathbf{x}_0 + \frac{\left(\mathbf{F}_1^0 - \mathbf{F}_2^0\right)}{\langle \nabla H_2^0, \mathbf{F}_2^0 \rangle} \left\langle \nabla H_2^0, \left( \mathbf{x}_0 - \mathbf{F}_1^0 \frac{\langle \nabla H_1^0, \mathbf{x}_0 \rangle}{\langle \nabla H_1^0, \mathbf{F}_1^0 \rangle} \right) \right\rangle + o(|\mathbf{x}_0|). \tag{2.10}$$

This then is the zero-time discontinuity mapping for trajectories that intersect the wedge. Taking into account trajectories that do not cross the wedge, the entire DM can be simplified to read

$$\mathbf{x} \to \begin{cases} \mathbf{x} & \text{if non-crossing,} \\ \mathbf{x} + (\mathbf{F}_1^0 - \mathbf{F}_2^0)\langle \mathbf{a}_2, \mathbf{x} \rangle + o(|\mathbf{x}|) & \text{if crossing,} \end{cases} \tag{2.11}$$

where

$$\mathbf{a}_2 = \mathbf{J}_2 - \langle \mathbf{J}_2, \mathbf{F}_1^0 \rangle \mathbf{J}_1, \qquad \mathbf{J}_i = \frac{\nabla H_i^0}{\langle \nabla H_i^0, \mathbf{F}_i^0 \rangle}. \tag{2.12}$$

**Remarks** Observe several properties of the ZDM (2.11).

1. To lowest order (2.11) is a piecewise-linear map, defined by matrices that are in general non-equal for crossing and non-crossing trajectories. Note that the matrix for crossing-trajectories is a rank one update of the identity. More precisely, a local co-ordinate basis $\mathbf{x} = (x_1, \ldots, x_n)$ can be chosen so that the $n^{th}$ co-ordinate axis points in the direction of $(\mathbf{F}_1^0 - \mathbf{F}_2^0)$. Then, the the ZDM for crossing trajectories takes the **normal form**

$$\mathbf{x} \to \begin{cases} \mathbf{x} & \text{if non-crossing,} \\ A\mathbf{x} & \text{if crossing,} \end{cases} \qquad \text{where} \quad A = \begin{bmatrix} 1 & 0 & \ldots & 0 & 0 \\ 0 & 1 & \ldots & 0 & 0 \\ \vdots & \vdots & \ldots & \vdots & \\ 0 & 0 & \ldots & 1 & 0 \\ a_{n,1} & a_{n,2} & \ldots & a_{n,n-1} & a_{n,n} \end{bmatrix} \tag{2.13}$$

   with the $a_{n,k}$ explicitly calculable in terms of $\mathbf{F}_i^0$ and $\nabla H_i^0$, $i = 1, 2$. This is precisely the form of the map used by Feigin to describe $C$-bifurcations (see di Bernardo, Feigin, Hogan & Homer (1999)).

2. The ZDM can clearly be seen to reduce to the identity map to lowest order when the two vector fields are equal at $\mathbf{x} = \mathbf{0}$.

3. Close examination of the definition of $\mathbf{a}_2$ reveals that the ZDM also reduces to the identity when the corner sharpens to the limit of having zero width, i.e when $\nabla H_1^0 = -\nabla H_2^0$. More precisely, this shows that corner collision with corner having a higher than linear contact, i.e. a cusp, will lead to maps that have continuous first derivatives. Presumably singularities would occur in higher derivatives of the map in this case.

4. Note that the above analysis not only shows that the linear approximation is valid for sufficiently small $\mathbf{x}$, but it also gives insight into the region of validity of the linear approximation. Specifically we needed to assume $\mathbf{x} \ll \max\{\langle \nabla H_i^0, \mathbf{F}_i^0 \rangle : i = 1, 2\}$. Hence if either of these two angles is small (e.g. when the vector field for system one makes a shallow angle with the first boundary $H_1 = 0$) then the range of $\mathbf{x}$ for which the linear map is valid will be small. The linear region will also clearly be small if either of the boundaries $H_1 = 0$ or $H_2 = 0$ is highly curved, as may be confirmed by taking more terms in the Taylor expansion of $H_1 = 0$ leading to (2.5).

5. Finally, note that the map ceases to be valid in the limit that the corner becomes flat, i.e. when $\nabla H_1^0 = \nabla H_2^0$, since the slope conditions (2.2) cannot be satisfied by any pair of vector fields. Instead one would have to assume $\langle \mathbf{F}_i^0, \nabla H_1^0 \rangle = 0$, $i = 1, 2$ which would be the conditions for a grazing with a smooth boundary. This would lead to a totally different form of ZDM. Note that in the limit of the corner becoming shallower towards a smooth boundary, then (2.2) imposes stronger and stronger restrictions on the vector fields $\mathbf{F}_1$ and $\mathbf{F}_2$ in order for a corner-collision to occur.

### 2.3 Poincaré-section discontinuity mapping (PDM)

The above ZDM is useful for studying periodic orbits via fixed time mappings, such as *stroboscopic* Poincaré maps in periodically forced systems. However, in general Poincaré maps are defined with respect to codimension-one surfaces that are transverse to the flow. In such cases, we have to consider a modification to the ZDM, to define the discontinuity map from within a Poincaré section while losing the restriction that the correction should take zero time. In order to do this, we choose a locally linear section $\Gamma$ and some local co-ordinates in the neighbourhood of the corner; $\mathbf{x} = (y, \mathbf{z})$, $y \in \mathbb{R}$, $\mathbf{z} \in \mathbb{R}^{n-1}$ such that $\Gamma := \{y = 0\}$, see Figure 4(b). Note that the slope conditions (2.2) ensure such a $\Gamma$ may always be chosen so that it is transverse to both $\phi_1$ and $\phi_2$. (In fact, in order to compare the resulting Poincaré maps with the full flow of the ODE system, it is often most convenient to choose $\Gamma$ to be one of the surfaces $\nabla H_1 = 0$ or $\nabla H_2 = 0$, which automatically satisfy transversality due to the slope conditions — see the examples in Section 5 below). In what follows we do not make this simplification, which would make either $t_1$ or $t_3$ defined below be precisely zero, but stick instead to a more general analysis which of course includes these special cases.)

Now, with reference to Figure 4(b), we want to

- solve system 1 starting at $\mathbf{x} = \mathbf{x}_0 = (0, \mathbf{z}_0)$ for time $-t_1$ until $\mathbf{x} = \mathbf{x}_1$ such that $H_1(\mathbf{x}_1) = 0$,
- then solve system 2 for time $s_2$ until $\mathbf{x} = \mathbf{x}_2$ such that $H_2(\mathbf{x}_2) = 0$,
- and finally solve system 1 again for time $-t_3$ until $\mathbf{x} = \mathbf{x}_3 = (y_3, \mathbf{z}_3)$ where $y_3 = 0$.

The analysis proceeds similarly to the ZDM case, with again a linear approximation to the flow proving to be sufficient. It is helpful to ease notation by defining $\mathbf{F}_i = (f_i, \mathbf{g}_i)$ so that

$$\phi_i((y, \mathbf{z}), t) = \left(y + f_i^0 t + o(y, |\mathbf{z}|),\ \mathbf{z} + \mathbf{g}_i^0 t + o(y, |\mathbf{z}|)\right),$$

where the transversality of $\Gamma$ implies that $f_i^0 \neq 0$, $i = 1, 2$. Then $t_1$ and $\mathbf{x}_1 = (y_1, \mathbf{z}_1)$ are defined as before by (2.6) and (2.7) where in particular $y_1 = -f_1^0 T_1(0, \mathbf{z}_0) + o(\mathbf{z_0})$, and $s_2$ and $\mathbf{x}_2$ are again

given by (2.8) and (2.9). The difference now comes with the definition of $\mathbf{x}_3$ and the unknown time $t_3$. These are defined by the unique local solution $T_3(\mathbf{x}_2)$ and $\mathbf{z}_3$ of

$$\mathbf{x}_3 = (0, \mathbf{z}_3) = \phi_1(\mathbf{x}_2, -T_3(\mathbf{x}_2)) = \left(y_2 - f_1^0 T_3(\mathbf{x}_2) + o(y_2, |\mathbf{z}_2|),\ \mathbf{z}_2 - \mathbf{g}_1^0 T_3(\mathbf{x}_2) + o(y_2, |\mathbf{z}_2|)\right). \tag{2.14}$$

From the first equation of (2.15) we obtain

$$T_3(\mathbf{x}_2) = (y_2/f_1^0) + o(y_2, |\mathbf{z}_2|),$$

and hence from the second equation

$$\mathbf{z}_3 = \mathbf{z}_2 - \mathbf{g}_1^0 (y_2/f_1^0) + o(y_2, |\mathbf{z}_2|).$$

Upon substitution from (2.6), (2.7), (2.8) and (2.9), this expression for $\mathbf{z}_3$ can be rearranged to read

$$\mathbf{z}_3 = \mathbf{z}_0 + \frac{\left(\mathbf{g}_1^0 \frac{f_2^0}{f_1^0} - \mathbf{g}_2^0\right)}{\langle \nabla H_2^0, \mathbf{F}_2^0 \rangle} \left( \langle \nabla H_2^0, \mathbf{x}_0 \rangle - \frac{\langle \nabla H_2^0, F_1^0 \rangle}{\langle \nabla H_1^0, F_1^0 \rangle} \langle \nabla H_1^0, \mathbf{x}_0 \rangle \right) + o(|\mathbf{z}_0|), \tag{2.15}$$

where $\mathbf{x}_0 = (0, \mathbf{z}_0)$. Like the ZDM, the PDM can now be simplified to read

$$\mathbf{z} \to \begin{cases} \mathbf{z} & \text{if non-crossing,} \\ \mathbf{z} + (\mathbf{g}_1^0 \frac{f_2^0}{f_1^0} - \mathbf{g}_2^0) \langle \mathbf{a}_2^*, \mathbf{z} \rangle + o(|\mathbf{x}|) & \text{if crossing,} \end{cases} \tag{2.16}$$

where $\mathbf{a}_2^* \in \mathbb{R}^{n-1}$ is a vector composed of the final $n-1$ components of $\mathbf{a}_2$ defined by (2.12).

The PDM has all the properties of the ZDM given in remarks 1–5 above, the only difference being that it is defined on a Poincaré section so it maps

$\Gamma \subset \mathbb{R}^{n-1} \to \mathbb{R}^{n-1}$ instead of $\mathcal{D} \subset \mathbb{R}^n \to \mathbb{R}^n$.

# 3 The global Poincaré map

Now let us suppose that the system (2.1) depends smoothly on a parameter $\mu$, and that at $\mu = 0$ there is a periodic orbit $\mathbf{x}(t) = \mathbf{p}(t)$ that grazes with the corner at the point $\mathbf{x} = \mathbf{0} = \mathbf{p}(0)$ (where the phase of $\mathbf{p}$ has been fixed without loss of generality). Moreover we shall assume that this orbit is hyperbolic and hence isolated (we shall not consider the Hamiltonian case here). Finally, we assume that if $\mathbf{p}$ crosses any other discontinuity boundaries $\Sigma'$ outside of the region $\mathcal{D}$, then it does so at points where $\Sigma'$ is smooth and it does so transversally. That is there are no points of grazing or corner-collision along $\mathbf{p}(t)$ other than at $t = 0$. Moreover since these are both open conditions, then we assume that they are true for a sufficiently small neighbourhood of $\mu = 0$ and $\mathbf{p}(t)$.

Consider first the case of a non-autonomous system whose coefficients are periodic with period $T$. We are thinking here of the case of a forced oscillator system, for example. Then suppose that $\mathbf{p}(t)$ is an $mT$-periodic orbit for some $m > 0$. Hence, for $\mu = 0$, $\mathbf{x} = \mathbf{0}$ will a fixed point of the time-$mT$ flow map $\Pi_{per}$ defined, in a full neighbourhood of $\mathbf{x} = \mathbf{0}$, by solving the flow in a neighbourhood of $\mathbf{p}(t)$ as if region $S_2$ were empty and $\phi_1$ applied throughout $\mathcal{D}$. The assumptions on smooth parameter dependence, hyperbolicity and lack of further grazing or corner-collisions outside $\mathcal{D}$ then imply generically that

$$\Pi_{per} : \mathbf{x} \mapsto P\mathbf{x} + \mathbf{q}\mu + o(|\mathbf{x}|, \mu), \tag{3.1}$$

for some nonsingular $n \times n$ matrix $P$ and non-zero $n$-dimensional vector $\mathbf{q}$. For simplicity, we assume the ZDM (2.11) to be $\mu$-independent without loss of generality, since one can perform a local parameter-dependent change of co-ordinates if necessary. A global time-$mT$ map can be

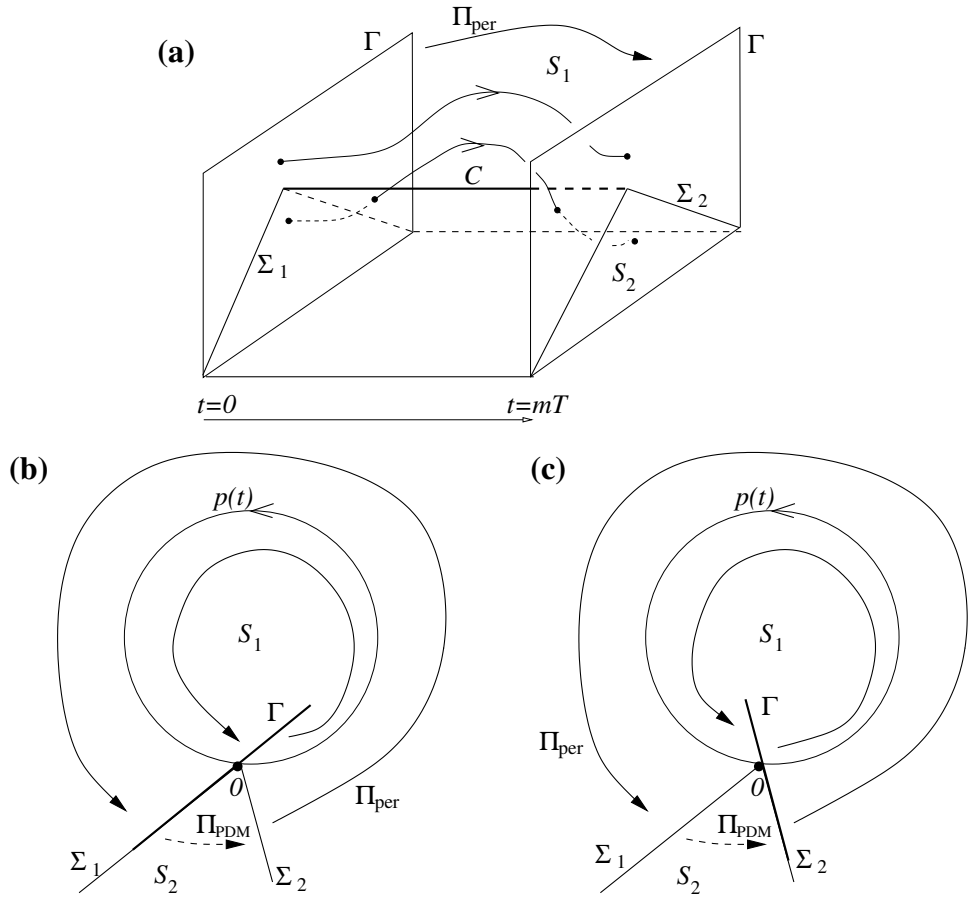


Figure 5: *Illustrating qualitatively the construction of global Poincaré maps. In (a) the time-dependent case is illustrated. Then either of the maps* (3.2) *or* (3.3) *depending on whether the adjustment (the ZDM) made for passage through $S_2$ is made at $t = 0$ or $t = mT$. Panels (b) and (c) illustrate the general case where the Poincaré section $\Gamma$ is chosen to be either $\Sigma_1$ or $\Sigma_2$, leading respectively to the maps* (3.5) *or* (3.6)

obtained by composing the ZDM with $\Pi_{per}$. Note that for comparison with numerical results it may be beneficial to express the resulting global map in one of two equivalent ways:

$$\Pi_{per} \circ \Pi_{ZDM} : \quad \mathbf{x} \to \begin{cases} P\mathbf{x} + \mathbf{q}\mu + o(|\mathbf{x}|, \mu) & \text{if non-crossing,} \\ P\left(\mathbf{x} + (\mathbf{F}_1^0 - \mathbf{F}_2^0)\langle \mathbf{a}_2, \mathbf{x}\rangle\right) + \mathbf{q}\mu + o(|\mathbf{x}|, \mu) & \text{if crossing,} \end{cases} \tag{3.2}$$

$$\Pi_{ZDM} \circ \Pi_{per} : \quad \mathbf{x} \to \begin{cases} P\mathbf{x} + \mathbf{q}\mu + o(|\mathbf{x}|, \mu) & \text{if non-crossing,} \\ P\mathbf{x} + (\mathbf{F}_1^0 - \mathbf{F}_2^0)\langle \mathbf{a}_2, (P\mathbf{x} + \mathbf{q}\mu)\rangle + \mathbf{q}\mu + o(|\mathbf{x}|, \mu) & \text{if crossing.} \end{cases} \tag{3.3}$$

See Figure 5(a). Either of these maps then describes all trajectories that remain within a neighbourhood of the corner-colliding periodic orbit; a fixed point represents an $mT$-periodic orbit of the flow, period-$n$ points represent $mnT$-periodic orbits, etc. Again note that either version of the map is precisely of the form studied by Feigin, and by Nusse and co-workers, which are known to undergo a rich variety of bifurcation phenomena as $\mu$ is varied, such as period-multiplying and sudden jumps to chaos, as mentioned in the Introduction.

Now let us consider the more general case of an autonomous system, or a non-autonomous system with time taken to be one of the dynamical states. Here we shall use the Poincaré section $\Gamma$ defined in the previous section in terms co-ordinates local to the corner. Now we have no need for information on the period of the hyperbolic periodic orbit $\mathbf{p}(t)$, just that it represents the fixed point of a Poincaré map from $\Gamma$ to itself defined by the flow where $\phi_1$ applies throughout

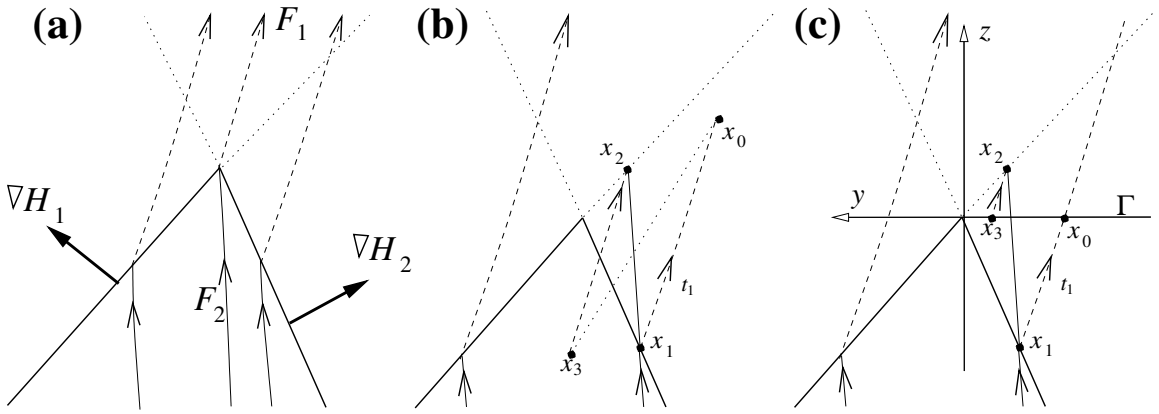


Figure 6: **(a)** *The geometry of the corner at an internal corner-collision.* **(b)**, **(c)** *The definition of ZDM and PDM respectively in analogy with Figure 4 for the external case.*

$\mathcal{D}$. The assumptions about hyperbolicity and no other grazings or corner-collisions along $\mathbf{p}$ mean that this Poincaré map generically takes the form

$$\Pi^*_{per} : \mathbf{z} \mapsto P^*\mathbf{z} + \mathbf{q}^*\mu + o(|\mathbf{z}|, \mu), \tag{3.4}$$

for some nonsingular $(n-1) \times (n-1)$ matrix $P^*$ and non-zero $(n-1)$-dimensional vector $\mathbf{q}^*$. In order to account for the correction owing to the portions of trajectories that enter $S_2$ in a neighbourhood of the corner, we must compose $\Pi^*$ with the PDM (2.16) to obtain a global Poincaré map. Again this can be done in two equivalent ways:

$$\Pi_{per} \circ \Pi_{PDM} : \quad \mathbf{z} \to \begin{cases} P^*\mathbf{z} + \mathbf{q}^*\mu & \text{if non-crossing,} \\ P^*\left(\mathbf{z} + (\mathbf{g}_1^0 \frac{f_2^0}{f_1^0} - \mathbf{g}_2^0)\langle \mathbf{a}_2^*, \mathbf{z}\rangle\right) + \mathbf{q}^*\mu + o(|\mathbf{z}|) & \text{if crossing,} \end{cases} \tag{3.5}$$

$$\Pi_{PDM} \circ \Pi_{per} : \quad \mathbf{z} \to \begin{cases} P^*\mathbf{z} + \mathbf{q}^*\mu & \text{if non-crossing,} \\ P^*\mathbf{z} + (\mathbf{g}_1^0 \frac{f_2^0}{f_1^0} - \mathbf{g}_2^0)\langle \mathbf{a}_2^*, (P^*\mathbf{z} + \mathbf{q}^*\mu)\rangle + \mathbf{q}^*\mu + o(|\mathbf{z}|) & \text{if crossing.} \end{cases} \tag{3.6}$$

These maps have the same general form as (3.2) and (3.3) but are defined from the codimension-one surface $\Gamma$ to itself. Note that (3.5) applies most naturally to the case where the Poincaré section $\Gamma$ is chosen to be $\Sigma_1 := \{H_1 = 0\}$, i.e. the boundary of entry into the wedge $S_2$, whereas (3.6) applies most naturally when $\Gamma = \Sigma_2 := \{H_2 = 0\}$, the point of exit from the wedge. See Figure 5(b).

# 4 The internal grazing case

Now consider the case of internal grazing, as in Figure 2(b). Here a local analysis in a neighbourhood of the corner must be different since all trajectories spend time in both regions $S_1$ and $S_2$. However, the DM in this case fulfills a different function. It no longer describes the correction that must be added to trajectories that always remain in $S_1$ in order to describe the local effect of trajectories that intersect the wedge $\Sigma$. Instead we will define a DM that computes the correction for trajectories that intersect $\Sigma$ to the right-hand side of the corner (i.e. along $\{H_2 = 0\}$) in order to solve the global Poincaré map as if the corner were not there and all trajectories crossed the continuation into $S_1$ of the left-hand boundary $\{H_1 = 0\}$. See Figure 6.

First we note that the necessary conditions (2.2) must change for an internal grazing, namely we must have (without loss of generality, up to a reversal of time if necessary)

$$\langle \mathbf{F}_i, \nabla H_1\rangle > 0, \quad \langle \mathbf{F}_i, \nabla H_2\rangle > 0, \quad \text{for} \quad i = 1, 2. \tag{4.1}$$

Next, notice the similarity between Figure 6(b),(c) and Figure 3 which define the local discontinuity mappings for the internal and external cases respectively. In fact, the geometry of the DMs in the two cases are identical up to rotation of the external case through 90° anti-clockwise. Hence the arguments of Sections 2 and 3 can be repeated word for word, after the re-definition of various quantities. In particular, the role of the wedge gets replaced by the thick portion of the boundary $H_2$ and the continuation of $H_1$ beyond the corner. For this new virtual wedge, we must assume that vector field $\mathbf{F}_1$ applies *inside* the wedge and $\mathbf{F}_2$ *outside*; hence the roles of two vector fields are swapped. Also, the geometry shows that $-\nabla H_2$ plays the role previously played by $\nabla H_1$ and $\nabla H_1$ replaces $\nabla H_2$. Note also from Figure 6 that, for the PDM, the Poincaré section has to be appropriately redefined in order to satisfy transversality.

Having made these alternations we can now write down the global Poincaré maps for the internal case directly. For the zero-time Poincaré map we therefore obtain

$$\mathbf{x} \to \begin{cases} P\mathbf{x} + \mathbf{q}\mu + o(|\mathbf{x}|, \mu) & \text{if non-crossing,} \\ P\left(\mathbf{x} + (\mathbf{F}_2^0 - \mathbf{F}_1^0)\langle \mathbf{a}_1, \mathbf{x}\rangle\right) + \mathbf{q}\mu + o(|\mathbf{x}|, \mu) & \text{if crossing,} \end{cases} \tag{4.2}$$

and for the Poincaré section version

$$\mathbf{z} \to \begin{cases} P^*\mathbf{z} + \mathbf{q}^*\mu & \text{if non-crossing,} \\ P^*\left(\mathbf{z} + (\mathbf{g}_2^0 \frac{f_1^0}{f_2^0} - \mathbf{g}_1^0)\langle \mathbf{a}_1^*, \mathbf{z}\rangle\right) + \mathbf{q}^*\mu + o(|\mathbf{z}|) & \text{if crossing.} \end{cases} \tag{4.3}$$

Here

$$\mathbf{a}_1 = \mathbf{J}_1 - \langle \mathbf{J}_1, \mathbf{F}_2^0\rangle \mathbf{J}_2, \qquad \mathbf{J}_i = \frac{\nabla H_i^0}{\langle \nabla H_i^0, \mathbf{F}_i^0\rangle},$$

and all other quantities are defined similarly to the external case. Note that we have only written down the maps corresponding to $\Pi_{per} \circ \Pi_{DM}$, the equivalent maps obtained from taking the opposite order of composition are obvious.

Note in the above that there was an arbitrariness in whether we chose to define the DM as correcting those trajectories that cross to the right of the corner (intersecting $H_2$) in order to describe solutions by the global Poincaré map associated with trajectories that cross to the left (intersecting $H_1$), which we did, or vice versa. Of course the two maps would be equivalent, with the difference in the functional form of the maps being absorbed in the fact that $P$ and $\mathbf{b}$ would be defined differently. In one case, they will describe the linearization for periodic orbits that remain locally to the left of the corner, and in the other case describe linearization around periodic orbits that are to the right. For the maps given above, $P$ and $\mathbf{b}$ must be interpreted as the linearization around periodic orbits that cross $H_1$.

# 5 Examples

In order to illustrate the preceding theory, we shall consider two example systems and calculate explicitly the discontinuity mappings for periodic orbits that graze with a corner in the discontinuity set. These calculations will then be compared with equivalent maps formed by solving the system equations directly. In each case we shall show the effect the corner collision has on the existence of periodic orbits that are simple fixed points of the ensuing Poincaré maps. In fact, in both cases, we can show that there is a sharp corner in the bifurcation diagram of such one-periodic orbits. However a complete investigation of the dynamics generated by these Poincaré maps is left for future work.

## 5.1 A simple two-dimensional example

We consider first an example where a hyperbolic limit cycle grazes with a corner in an autonomous, piecewise-smooth vector field that is soluble in closed from. Specifically we take a

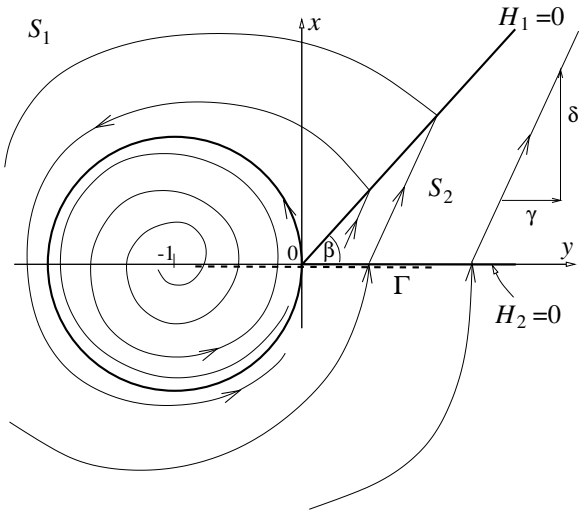


Figure 7: *Sketch of the phase portrait of* (5.1), (5.2) *with* $a = 1$

system

$$\begin{array}{rcl} \dot{x} &=& \gamma \\ \dot{y} &=& \delta \end{array} \quad , \quad \text{for } x > 0,\ y > 0,\ y < x\tan\beta \quad (\text{REGION } S_2), \tag{5.1}$$

$$\begin{array}{rcll} \dot{r} &=& \varepsilon r(a-r) & \\ \dot{\theta} &=& 0 & \end{array} \quad , \quad \text{otherwise (REGION } S_1); \quad \text{where} \quad x+1 = r\cos\theta,\ y = r\sin\theta. \tag{5.2}$$

Here $\gamma$, $\delta$, $\beta$, $\varepsilon$ and $a$ are real constants satisfying the constraints

$$0 < \beta < \pi/2, \quad \delta > \gamma\tan\beta. \tag{5.3}$$

See Figure 7. The system (5.2) is the normal from of a Hopf bifurcation occuring for $a = 0$. For $a > 0$ there is a limit cycle which is stable if $\varepsilon > 0$. At $a = 1$ this limit cycle collides with the boundary of region 2 in an external corner collision bifurcation. Specifically we take

$$H_1(x,y) = y, \quad H_2(x,y) = y\cos\beta - x\sin\beta.$$

The constraints (5.3) ensure that the slope conditions (2.2) are satisfied along $H_1 = 0$ and $H_2 = 0$.

Since the systems in regions 1 and 2 are solvable in closed form one can explicitly construct the Poincaré map $x_0 \mapsto \Pi x_0$ associated with the Poincaré section $\{y = 0, x > -1\}$, and this can then be compared with the global Poincaré map (3.5) from the theory. In region 1 the general solution takes the form

$$r(t) = \frac{a r_0 \exp(-\varepsilon a t)}{r_0\exp(-\varepsilon a t) + a - r_0}, \quad \theta = \theta_0 + t. \tag{5.4}$$

For $x_0 < 0$ ($r_0 < 1$), this equation defines the Poincaré map after setting $r_0 = x_0 + 1$, $\theta_0 = 0$ and $t = 2\pi$. For $x_0 > 0$, however, we must first solve (5.1) until the time

$$\hat{t} = \frac{x_0\tan\beta}{\delta - \gamma\tan\beta} \tag{5.5}$$

at which $y = x\tan\beta$. Taking the $(x,y)$-values at this point, converting to polar co-ordinates $(\hat{r},\hat{\theta})$ where

$$\hat{r}\cos\hat{\theta} = x_0 + \gamma\,\hat{t} - 1, \quad \hat{r}\sin\hat{\theta} = \delta\,\hat{t}, \tag{5.6}$$

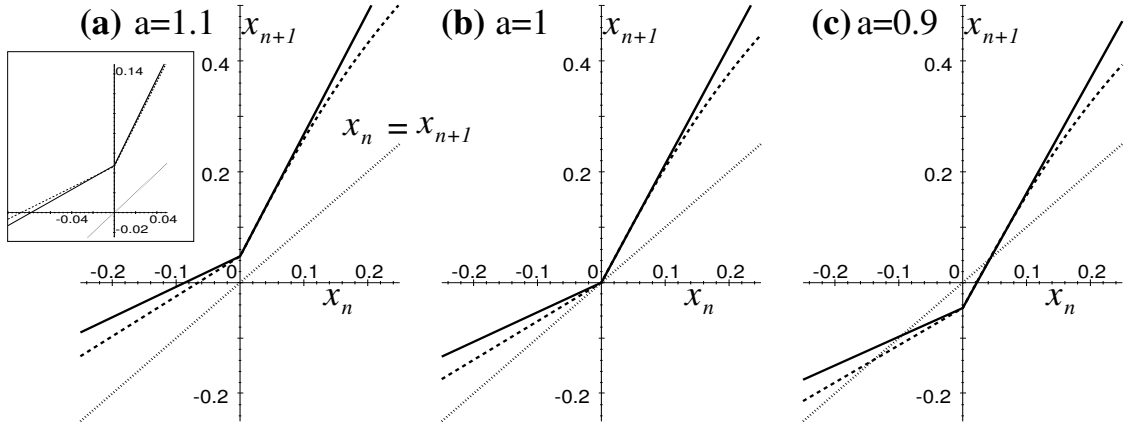


Figure 8: Comparison between the PDM given by (5.10) (solid line) with the map obtained from the exact analytical solution of (5.1), (5.2) (dashed line). (Note that there is agreement between the slopes of the two maps on either side of $x_n = 0$. For $x_n < 0$, this agreement is not so obvious but it has been confirmed for *each* of the three $a$-values by plotting the graphs on a shorter $x_n$-interval. Just such a zoom for $a = 1.1$ is depicted as an inset to (a).) Intersection of the map with the dotted line represents the existence of a fixed point. Numerical values used are $\varepsilon = 1/10$, $\beta = \pi/4$, $\gamma = 3/8$, $\delta = 1/2$ and the three given values of $a$.

substituting these values as $r_0$ and $\theta_0$ in (5.4) and evaluating at $t = 2\pi - \hat{t}$ then us gives an analytic expression for the Poincaré map for $x_0 > 0$. Thus we obtain

$$x_0 \to \frac{a\hat{r}\exp[-\varepsilon a(2\pi - \hat{t})]}{\hat{r}\exp[-\varepsilon a(2\pi - \hat{t})] + a - \hat{r}}, \quad x_0 > 0, \tag{5.7}$$

where $\hat{t}$ and $\hat{r}$ are related to $x_0$ via (5.5) and (5.6).

This exact map may be compared to the global PDM (3.5), taking $\mu = a - 1$, for which it is easily calculated that

$$f_1^0 = 1,\ f_2^0 = \delta,\ g_1^0 = 0,\ g_2^0 = \gamma, \nabla H_1^0 = (0, -1),\ \nabla H_2^0 = (-\sin\beta, -\cos\beta) \tag{5.8}$$

Moreover, $P^*$ and $\mathbf{q}^*\mu$ can be calculated from the first terms of the Taylor expansion in $r_0 - 1$ and $a - 1$ respectively of the solution of $r(2\pi)$ given by (5.4), evaluated at $a = 1$. From this we obtain

$$P^* = \exp(-2\varepsilon\pi), \quad \mathbf{q}^*\mu = (1 - \exp(-2\varepsilon\pi))(a - 1). \tag{5.9}$$

Note that since we take the Poincaré section $\Gamma$ to be equal to $\{H_2 = 0\}$, the comments at the end of Section 3 dictate that we should take the global PDM given by (3.5), which using (5.8) and (5.9) is easily calculated to be

$$x_0 \to \begin{cases} \exp(-2\varepsilon\pi)x_0 + (1 - \exp(-2\varepsilon\pi))(a - 1) & \text{if} \quad x_0 < 0 \\ \delta\,[\exp(-2\varepsilon\pi)/(\delta - \gamma\tan\beta)] + (1 - \exp(-2\varepsilon\pi))(a - 1) & \text{if} \quad x_0 > 0 \end{cases} \tag{5.10}$$

Figure 8 gives the comparison between the PDM and the exact map. Note both the qualitative and quantitative agreement between the two. Note also that for the illustrated numerical values of the various constants, the corner-collision has the effect of destroying the limit cycle. Before the bifurcation, i.e. for $a < 1$, there is the stable limit cycle lying solely in region 1, but this coexists with an unstable limit cycle which passes through region 2. At $a = 1$ these two periodic solutions coalesce and for $a > 1$ they have disappeared. Note finally that unlike a saddle-node bifurcation for a smooth system, the Floquet multipliers of the two periodic orbits (the slopes of the two portions of the map) do not approach 1 as $a \to 1^-$.

## 5.2 The buck converter

DC-DC buck converters are a form of piecewise-linear circuit used widely in power electronics for adjusting a given DC voltage to a lower value. Here we shall take the form of the equations modelling such a circuit used in di Bernardo et al. (1998) which are written in terms of a current $I(t)$ and voltage $V(t)$

$$\dot{V} = -\frac{1}{RC}V + \frac{I}{C} \tag{5.11}$$

$$\dot{I} = -\frac{V}{L} + \begin{cases} 0 & V \geq V_r(t) \\ E/L & V < V_r(t). \end{cases} \tag{5.12}$$

Here $C$, $E$, $L$ and $R$ are positive constants representing a capacitance, battery voltage, inductance and resistance respectively and $V_r$ is a piecewise-linear but discontinuous reference 'ramp' signal

$$V_r(t) = \gamma + \eta(t \bmod T), \qquad \gamma,\ \eta,\ T > 0.$$

For this system we have $\Sigma := \{V = V_r(t)\}$ which has corners whenever $t = 0 \bmod T$.

The reader is referred to di Bernardo et al. (1998) and references therein for details of the electrical circuit represented by the model (5.11),(5.12) and for some of the rich features of its dynamics. These features include periodic orbits and strange attractors that are characterized by trajectories that are close to both corner-collision (at $t = 0 \bmod T$) and sliding (with $V(t) = V_r(t)$ for $(m-1)T < t < mT$ for some $m$). The parameter values taken were those used in the experiments of Deane & Hamill (1990), which in SI units are

$$R = 22\Omega,\ C = 4.7\mu F,\ L = 20mH,\ T = 400\mu s,\ \gamma = 11.75238V,\ \eta = 1309.524Vs^{-1}, \tag{5.13}$$

with the bifurcation parameter $E \in (15, 60)$ being the input voltage.

In this paper we shall limit ourselves to an analytical explanation of the phenomenon that was merely observed numerically in di Bernardo et al. (1998) namely that corner-collision of a periodic orbit is described by a piecewise-linear map. Moreover the dynamics of this map are such that it causes a fold (actually a sharp corner) in the bifurcation diagram of a branch of periodic orbits. Specifically a sequence of such folds was found for certain 3T and 5T-periodic orbits, as part of a bigger picture of a spiraling bifurcation diagram; see also (Fossas & Olivar 1996). The origin of the spiral was explained in terms of a local analysis close to a (codimension-two) sliding periodic orbit, but the missing analytical ingredient in the explanation of the spirals was that corner-collision bifurcation causes the folds. What we shall show here, using the preceding analysis, is that by simply calculating a few features of the single trajectory undergoing the corner collision one can calculate precisely the angle of the fold in the bifurcation diagram and determine the stability of orbits.

Note the contrast with the work of Yuan et al. (1998) for a related buck-converter configuration. They *assume a priori* that the map associated with a corner-collision is piecewise linear. They then create a good match with the normal forms for such maps analysed by Nusse et al. (1994) by simply calculating the Jacobian of the flow for periodic orbits that are on *both* sides of the corner-collision. In contrast, our analysis *proves* that the appropriate map is piecewise-linear and we will show how to calculate it in terms of linearization about the *single* orbit that undergoes collision.

Suppose that at some $E = E_0$, an $nT$ periodic-orbit for some $n > 1$ collides with the upper corner of the function $V_r(t)$ at

$$t = t_0 = 0 \bmod T, \quad V = \gamma + \eta T, \quad I = I_0,$$

for some $I_0$ representing the value of current as the periodic trajectory crosses the corner. Moreover, (see Figure 9) we will consider the possibility of both internal and external corner collision.

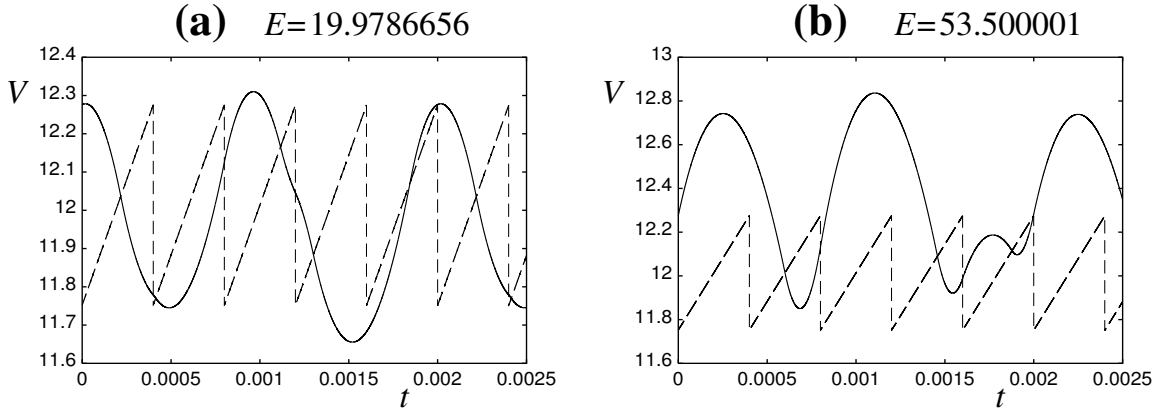


Figure 9: *Periodic orbits of the DC/DC buck converter with period* $5T$ *undergoing* **(a)** *an external and* **(b)** *an internal corner collision.*

As a first step, we define local co-ordinates

$$x = V - (\gamma + \eta T), \quad y = I - I_0, \quad z = t - t_0 \tag{5.14}$$

and rewrite the equation (5.11),(5.12) in autonomous form, to give the system

$$\begin{aligned} \dot{x} &= -a_1 + b_1 x - c_1 y, \\ \dot{y} &= -a_2 \qquad - c_2 y + dH(\sigma(z) - x), \\ \dot{z} &= 1, \end{aligned}$$

in which

$$a_1 = \frac{\gamma + \eta T - RI_0}{RC},\ b_1 = \frac{1}{C},\ c_1 = \frac{1}{RC}, a_2 = \frac{\gamma + \eta T}{L},\ c_2 = \frac{1}{L},\ d = \frac{E}{L}$$

$H$ is the Heaviside step function and

$$\sigma(z) = \eta[(z \bmod T) - T].$$

For this system we have

$$\Sigma_1 := \{H_1 = 0\} = \{x = \sigma(t)\}, \quad \Sigma_1 := \{H_2 = 0\} = \{z = 0\}, \quad \mathcal{C} = \{x = 0, z = 0\}.$$

The corner-collision happens at $x = y = z = 0$, and it can be checked that the conditions of the preceding theory are met there.

Now we can apply either the ZDM or PDM (with Poincaré section $z = 0$) in order to calculate the local effect of trajectories that are close to corner collision. It is trivial to check that both lead to the same results in this case since $z$ is really a time co-ordinate. Note that we have to include $z$ as a dynamical variable though, since the corner exists in the $(z, y)$-plane. Looking at the form of the ZDM (2.11), we have in this case

$$\nabla H_1^0 = (-1, 0, \eta), \quad \nabla H_2^0 = (0, 0, 1),$$

$$\mathbf{F}_1^0 = (-a_1, -a_2, 1), \quad \mathbf{F}_2^0 = (-a_1, -a_2 + d, 1)$$

(observe that $\mathbf{F}$ is discontinuous only in the $x$-direction, and so the jump in derivate of solutions is not seen in graphs of $y$ against $t$ as in Figure 9). Hence for an *external grazing*

$$\mathbf{J}_1 = \frac{1}{(a_1 + \eta)}(-1, 0, \eta), \quad \mathbf{J}_2 = (0, 0, 1), \quad \langle \mathbf{J}_2, \mathbf{F}_1^0 \rangle = 1.$$

Thus

$$\mathbf{a}_2 = \frac{1}{a_1 + \eta}(\eta, 0, \eta a_2)$$

and the ZDM for corner crossing trajectories takes the form

$$(x, y, z) \to (x, y, z) + (0, k_1 x + k_2 z, 0) + \text{ h.o.t},$$

where

$$\begin{aligned} k_1(E) &= -d\eta a_1 + \eta = -\frac{E\,RC}{L(\gamma + \eta T - RI_0 + \eta RC)} \\ k_2(E) &= -da_1 a_1 + \eta = -\frac{E(\gamma + \eta T - RI_0)}{L\gamma + \eta T - RI_0 + \eta RC}\,. \end{aligned} \tag{5.15}$$

However, since we are interested in a zero-time map, we can assume that $z = 0$ and hence we get a local mapping

$$\Pi_{ZDM} : \begin{pmatrix} x \\ y \end{pmatrix} \to \begin{pmatrix} x \\ y + k_1(E)x \end{pmatrix} + \text{ h.o.t.} \tag{5.16}$$

Note that this map depends on the bifurcation parameter $E$.

For internal grazing, we must use the formula (4.2) to calculate the ZDM. However, note that $\langle J_1, F_2 \rangle = 1 = \langle J_2, F_1 \rangle$ and hence the ZDM for the internal case is *identical* to that for the external case since $\mathbf{a}_1 = -\mathbf{a}_2$. Hence the zero-time local Poincaré map (with $z = 0$) is also given by (5.16) in this case.

We must next compose the map $\Pi_{ZDM}$ with a global one which is simply found by taking the Jacobian derivative of the flow around the periodic orbit at $E = E_0$ ignoring the effects of the corner

$$\Pi_{per} : \begin{pmatrix} x \\ y \end{pmatrix} \to A \begin{pmatrix} x \\ y \end{pmatrix} + \mathbf{b}(E - E_0), \tag{5.17}$$

where the coefficients of the matrix $A$ and vector $\mathbf{b}$ must in general be calculated numerically for particular periodic orbit undergoing corner collision. It is in the evaluation of $A$ that the difference between internal and external cases will be seen.

The time-$5T$ map is applied from the end of the ramp cycle $t = 0(\mod 5T)$, which implies $z = 0$ there, which is the definition of the Poincaré section $\{H_2 = 0\}$. Hence it make sense to use the second form of the global map (3.3) derived in Section 4, that is $\Pi_{ZDM} \circ \Pi_{per}$. In the external case, this map is simply $\Pi_{per}$ for trajectories that do not cross the ramp signal $x = \sigma(z)$ close to the corner. But for trajectories which do cross, it takes the form

$$\begin{pmatrix} x^{(n+1)} \\ y^{(n+1)} \end{pmatrix} = \begin{bmatrix} a_{11} & a_{12} \\ a_{21} + a_{11}k_1(E_0) & a_{22} + a_{12}k_1(E) \end{bmatrix} \begin{pmatrix} x^{(n)} \\ y^{(n)} \end{pmatrix} + \begin{pmatrix} b_{11} \\ b_{21} + k_1(E_0)b_{11} \end{pmatrix} (E - E_0), \tag{5.18}$$

where

$$A = \begin{bmatrix} a_{11} & a_{12} \\ a_{21} & a_{22} \end{bmatrix}, \quad \mathbf{b} = \begin{pmatrix} b_{11} \\ b_{21} \end{pmatrix}.$$

A similar reasoning shows the same map to hold for trajectories that intersect the corner to the left of $z = 0$ in the internal corner-collision case. For both cases the condition for the global map to be given by (5.18) rather than simply $\Pi_{per}$ is that the final voltage be less than the ramp, that is

$$\text{if} \quad x^{(n+1)} := a_{11}x^{(n)} + a_{12}y^{(n)} + b_{11}(E - E_0) < 0 \tag{5.19}$$

Now let us compare the predictions of this map with two different corner-colliding periodic orbits, one internal one external, of period $5T$ that are depicted in Figure 9. First we treat the external corner-colliding $5T$-periodic orbit that was numerically found to occur for

$$E = E_0 = 19.9786656, \quad I_0 = 0.56929860.$$

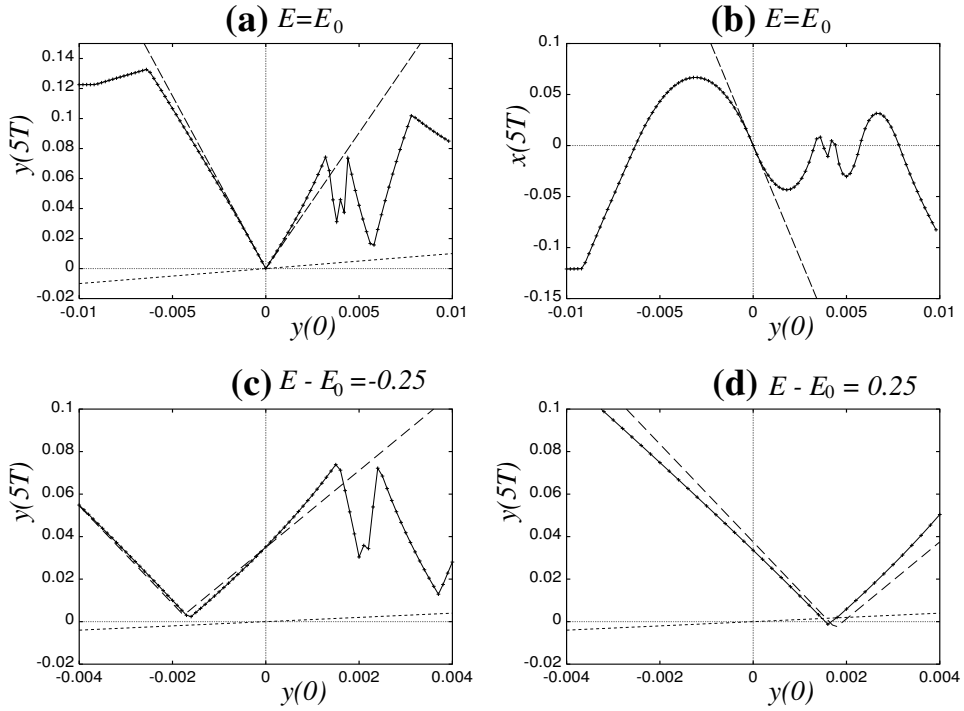


Figure 10: *The Poincaré map for a $5T$-periodic external corner-colliding orbit at $E_0 = 19.9786656$, computed numerically (solid line with crosses) and via the corner-collision analysis (dashed line). A one-dimensional slice of the map is taken considering the effect of varying only the initial current $y(0)$.* **(a)** *and* **(b)** *depict the final current and voltage respectively for $E = E_0$;* **(c)** *and* **(d)** *show the effect on the final current of variation of the bifurcation parameter $E$. In the final current versus initial current figures, the $45°$ line is depicted as dotted; viewing the graphs as approximations of 1D maps, intersections with this line are indicative of nearby fixed points of the 2D map.*

From these data we calculate from (5.15) that

$$k_1(E_0) = -0.934\,.$$

By computing this trajectory over five periods and using numerical differencing to calculate derivatives (taking initial condition and parameter perturbation of the appropriate sign in order to relate to trajectories with $x^{(n+1)} < 0$), we find that

$$A = \begin{bmatrix} -3.96 & -44.0 \\ -2.03 & -23.0 \end{bmatrix}, \quad \mathbf{b} = \begin{pmatrix} 0.31 \\ 0.15 \end{pmatrix} \tag{5.20}$$

Figure 10 shows the result of substituting these numerical values into the analytical Poincaré map (5.17), (5.18), (5.19), and its comparison with a map calculated from straightforward numerical integration of trajectories. We have chosen to illustrate just a one-dimensional approximation to this two-dimensional map, by only displaying the effect of changes in initial current $y$. This is purely for illustrative convenience (similar results were found with other combinations of $x(0)$ and $y(0)$ varying as initial conditions), but note from the numerically evaluated coefficients of $A$ in (5.20), that initial variations of current $y$ have a much bigger effect (by a factor of about 10) than variations of voltage $x$.

The results in Figure 10 (a) and (b) show good quantitative and qualitative agreement between the local theory and the numerics at $E = E_0$. They also illustrate the extent of the region of validity for the local analysis; for $-0.006 < y(0) < -0.0035$ at $E = E_0$, the local map is qualitatively correct, but outside of this region the numerical map shows extra corners. This is due to other corner-collisions taking place at $t = nT$ for some $n \leq 5$. Note from panels (b) in particular that there is no corner in the $x$ component of the numerically computed map — this component of the map is smooth — which is in complete agreement with the analytical result 5.18 (there is no change in the $x$-component).

Panels (c) and (d) show the effect of variation of $E$, with the existence of a fixed point on such a graph of $y(5T)$ against $y(0)$ being indicative only of a fixed point of the full 2D map. Here again there is good agreement between theory and numerics on how the map is perturbed as $E$ varies and that two fixed points (corresponding to unstable periodic orbits of the ODEs) are created at $E = E_0$ and coexist for $E > E_0$.

Next we treat an internal case, specifically the $5T$-periodic orbit that was found numerically to occur with

$$E = E_0 = 53.500001, \quad I_0 = 0.738109.$$

From these values and from numerical differencing (again taking perturbations on the correct side of the corner) applied to the numerically computed orbit we obtain

$$k_1(E_0) = 1.06, \quad A = \begin{bmatrix} -6.8 & -103 \\ 2.4 & 37.0 \end{bmatrix}, \quad \mathbf{b} = \begin{pmatrix} 0.24 \\ -0.083 \end{pmatrix}.$$

These values were substituted into the maps (5.17), (5.18), (5.19) and compared with the numerically simulated map, as was done in Figure 10 for the external case. The results are presented in Figure 11. A similarly good agreement between theory and numerics is found in this case too. Note that the internal grazing is such that the coefficients of the second row of $A$ are all positive, that $k_1$ is also positive, and $b_{21}$ is negative — the opposite signs to those for the external case. We have investigated other internal and external grazes occuring for $5T$-periodic orbits in the buck converter model (5.11), (5.12) at the parameter values (5.13) and found that these respective sign conditions hold for each. Moreover external corner collisions cause a pair of periodic orbits to be created for $E > E_0$ and internal ones for $E < E_0$. This internal graze investigated for $E_0 = 53.500001$ is the last such grazing found, upon increasing $E$, for periodic orbits of period $5T$. Note from Figure 11(c) and (d) that the corner in the graph of periodic solutions remains close to the 45° line and hence it is hard to predict whether the periodic orbits bifurcate for $E > E_0$ or $E < E_0$. More accuracy indicates that the latter holds.

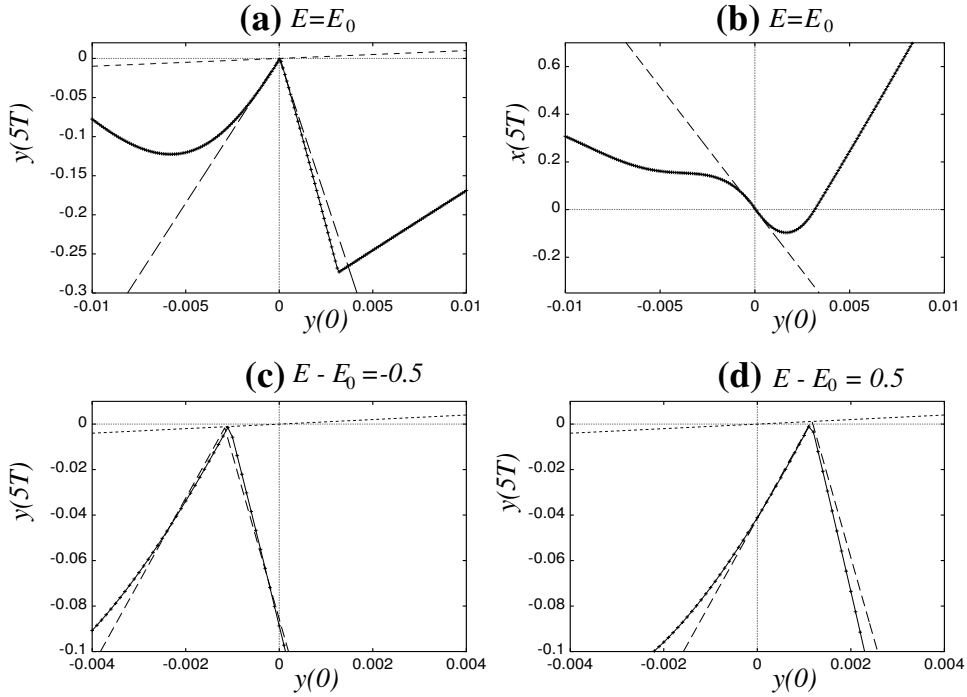


Figure 11: *Analogous to Figure 10, but for an internal corner collision at* $E_0 = 53.500001$.

# 6 Conclusion

In this paper we have presented for the first time a method for calculating the Poincaré map in a neighbourhood of a periodic orbit that grazes with the corner of a discontinuity boundary of a piecewise-continuous system of ODEs. It should be stressed that our analysis is purely local (as was amply demonstrated by Figures 10(a) and 11(a)) and it captures only the dynamics associated with trajectories that are sufficiently close to the corner-colliding one in both phase and parameter space. This is entirely equivalent to the situation for the analysis of periodic orbit local bifurcations in smooth systems of ODEs.

Nevertheless, the approach we take is quite general and leads to simple universal formulae which agree well with the computation of complete Poincaré maps for example systems. In particular we believe this to be the first direct proof that a codimension-one bifurcation in a class of ODE systems really does lead to maps that are piecewise-linear locally. Hence this is one situation were the beautiful theory of $C$-bifurcations, or border-collisions, for mappings applies directly to ordinary differential equations. In particular it should now be possible to find, or indeed construct, ODE examples of systems exhibiting robust chaos and many of the other complex bifurcation sequences known to occur for piecewise-linear maps. Also the method is likely to be useful to explain observed dynamical phenomena in other piecewise-smooth systems arising in applications, such as relay controllers and electrical or mechanical systems with saw-tooth forcing.

Finally, in this paper we have not investigated how the dynamics of the piecewise-linear maps we have derived; presumably the theory of Feigin and Nusse *et al.* can be brought to bear to classify the ensuing bifurcations of periodic solutions and strange attractors. Another outstanding issue for the two examples is the relation between the dynamics of piecewise-linear maps and the ODEs for which they are an approximation. Also, we have not considered the bifurcation caused by more complex invariant sets than periodic orbits undergoing corner collision. In di Bernardo et al. (1998) the jump from one-period-per-cycle to broad band chaos at $E \approx 32.342$ in the buck converter model of Section 5.2 was attributed numerically to just such a transition. All these

issues on the dynamical implications of our results are left for future work.

### Acknowledgements

MdiB acknowledges support from the Nuffield Foundation (scheme 'NUF-NAL') and the International Center for Advanced Studies in Nizhny Novgorod (INCAS- project no. 99-1-02). ARC acknowledges the support of the UK EPSRC with whom he holds an Advanced Fellowship.

## References

Banerjee, S. & Grebogi, C. (1999), 'Border collision bifurcations in two-dimensional piecewise smooth maps', *Physical Review E* **59**, 4052–4061.

Banerjee, S., York, J. & Grebogi, C. (1999), 'Robust chaos', *Physical Review E* **59**, 4052–4061.

Budd, C. & Dux, F. (1994), 'Chattering and related behaviour in impact oscillators', *Phil. Trans. Roy. Soc. Lond. A* **347**, 365–389.

Budd, C. & Dux, F. (1995), 'Intermittency in impact oscillators close to resonance', *Nonlinearity* **7**, 1191–1224.

Chin, W., Ott, E., Nusse, H. & Grebogi, C. (1994), 'Grazing bifurcations in impact oscillators', *Phys. Rev. E* **50**, 4427–4444.

Dankowitz, H. & Nordmark, A. (1999), 'On the origin and bifurcations of stick-slip oscillations', *Physica D* **136**, 280–302.

Deane, J. & Hamill, D. (1990), Analysis, simulation and experimental study of chaos in the buck concerter, *in* 'Proceedings of the Power Electronics Specialists Conf. (PESC 1990)', IEEE Press, New York, pp. 491–8.

di Bernardo, M., Budd, C. & Champneys, A. (1998), 'Grazing, skipping and sliding: analysis of the non-smooth dynamics of the DC/DC buck converter', *Nonlinearity* **11**, 859–890.

di Bernardo, M., Budd, C. & Champneys, A. (2000*a*), 'Local and global laws for grazing bifurcations in second-order forced oscillators'. Working document, in preparation.

di Bernardo, M., Budd, C. & Champneys, A. (2000*b*), 'A unified framework for studing grazings, border-collision and c-bifurcations'. Working document, in preparation.

di Bernardo, M., Feigin, M., Hogan, S. & Homer, M. (1999), 'Local analysis of $c$-bifurcations in $n$-dimensional piecewise-smooth dynamical systems', *Chaos Solitons and Fractals* **10**, 1881–1908.

di Bernardo, M., Johansson, K. H. & Vasca, F. (1999), Sliding orbits and their bifurcations in relay feedback systems, *in* 'Proc. 38th IEEE Conference on Decision and Control', Phoenix, AZ.

Feigin, M. (1970), 'Doubling of the oscillation period with $c$-bifurcation in piecewise continuous systems', *PMM* **34**, 861–869.

Filippov, A. (1988), *Differential equations with discontinuous righthand sides*, Kluwer, Dortrecht.

Fossas, E. & Olivar, G. (1996), 'Nb this reference to be swapped for the ijbc and for multiple pulsing paper: Study of chaos in the buck converter', *IEEE Trans. Circuits Sys. I: Fund. Th. Appl.* **43**, 13–25.

Lamba, H. (1995), 'Chaotic, regular and unbounded behaviour in the elastic impact oscillator', *Physica D* **82**, 117–135.

Nordmark, A. (1991), 'Non-periodic motion caused by grazing incidence in an impact oscillator', *J. Sound and Vibration* **145**, 279–297.

Nordmark, A. (1997), 'Universal limit mapping in grazing bifurcations', *Phys Rev E* **55**, 266–270.

Nusse, H. & Yorke, J. (1995), 'Border-collision bifurcations for piecewise smooth one-dimensional maps', **5**, 189–207.

Nusse, H., Ott, E. & Yorke, J. (1994), 'Border-collision bifurcation: An explanation for observed bifurcation phenomena', **49**, 1073–1076.

Shaw, S. & Holmes, P. (1983*a*), 'Periodically forced linear oscillator with impacts: chaos and long-periodic motions', *Phys. Rev. Lett.* **51**, 623–626.

Shaw, S. & Holmes, P. (1983*b*), 'A periodically forced piecewise linear oscillator.', *J. Sound and Vibration* **90**, 129–144.

Thompson, J. & Ghaffari, R. (1983), 'Chaotic dynamics of an impact oscillator', *Phys. Rev. A* **27**, 1741–1743.

Thompson, J. & Stewart, H. (1986), *Nonlinear Dynamics and Chaos; Geometric Methods for Engineers and Scientists*, Wiley, Chichester.

Thompson, J., Bokaian, A. & Ghaffari, R. (1983), 'Subharmonic resonances and chaotic motions of a bilinear oscillator', *IMA J. Appl. Math.* **31**, 207–234.

Yuan, G., Banerjee, S., Ott, E. & Yorke, J. (1998), 'Border-collision bifurcations in the buck converter', *IEEE Trans. Circ. Sys. I* **45**, 707–716.